Environmental Pollution 176 (2013) 123–133

Contents lists available at SciVerse ScienceDirect

Environmental Pollution

journal homepage: www.elsevier.com/locate/envpol

Modeling of air pollutant removal by dry deposition to urban trees using a WRF/CMAQ/i-Tree Eco coupled system

Maria Theresa I. Cabaraban [a,*], Charles N. Kroll [a], Satoshi Hirabayashi [b], David J. Nowak [c]

[a] Department of Environmental Resources Engineering, State University of New York, College of Environmental Science and Forestry, Syracuse, NY 13210, USA
[b] The Davey Tree Expert Company, 5 Moon Library, State University of New York, Syracuse, NY 13210, USA
[c] USDA Forest Service, Northern Research Station, Syracuse, NY 13210, USA

ARTICLE INFO

Article history:
Received 5 August 2012
Received in revised form
11 January 2013
Accepted 12 January 2013

Keywords:
Urban forestry
Meteorology
Air quality modeling
Dry deposition
Environmental quality

ABSTRACT

A distributed adaptation of i-Tree Eco was used to simulate dry deposition in an urban area. This investigation focused on the effects of varying temperature, LAI, and NO_2 concentration inputs on estimated NO_2 dry deposition to trees in Baltimore, MD. A coupled modeling system is described, wherein WRF provided temperature and LAI fields, and CMAQ provided NO_2 concentrations. A base case simulation was conducted using built-in distributed i-Tree Eco tools, and simulations using different inputs were compared against this base case. Differences in land cover classification and tree cover between the distributed i-Tree Eco and WRF resulted in changes in estimated LAI, which in turn resulted in variations in simulated NO_2 dry deposition. Estimated NO_2 removal decreased when CMAQ-derived concentration was applied to the distributed i-Tree Eco simulation. Discrepancies in temperature inputs did little to affect estimates of NO_2 removal by dry deposition to trees in Baltimore.

1. Introduction

Urban areas have become significant contributors of air pollution due to changes in transportation systems and industrial production (Gurjar et al., 2008; Hopke, 2009; Parrish et al., 2011). Air pollution can affect landscapes and ecosystems far from its source, thus its impact can be wide-reaching. Air pollutants are responsible for several adverse effects on human health, and can harm both the natural and the built environment (Davidson and Barnes, 2002; Driscoll et al., 2007; Schlesinger, 2007). In addition to reducing and controlling emissions, developing credible strategies to remove pollutants from the urban atmosphere is also of interest to air quality managers. An ecosystem approach, particularly the use of trees and shrubs for reducing air pollutants, should be an essential component of urban planning (Beckett et al., 1998; Freer-Smith et al., 2005).

Air pollutants are removed from the atmosphere through a variety of mechanisms, including precipitation scavenging (i.e. wet deposition), chemical reaction, and direct deposition to terrestrial and marine surfaces in the absence of precipitation (i.e. dry deposition). With vegetation, gaseous air pollutants are removed through dry deposition primarily by uptake via leaf stomata (Nowak et al., 2006). Depending on the chemical and physical properties of the gas and the absorbing surface, some gases are also removed by the plant surface (Smith et al., 2000). Trees can be significant sinks for gaseous pollutants since they provide a large surface (leaves, stems, barks) for pollutant uptake (Fowler, 2002).

Within the i-Tree modeling suite, i-Tree Eco (formerly known as the Urban Forest Effect model) is used to calculate air pollution removal by the urban forest and associated air quality improvement throughout the year (i-Tree, 2012). The dry deposition component of i-Tree Eco assumes that input hourly meteorological and air pollutant concentration data are homogeneous over a region, such that estimated pollutant removal rates are for the entire urban area modeled. Local influences of urban trees cannot be estimated and potential tree-planting sites would be challenging to identify using current i-Tree Eco techniques. The location of trees is important, as air pollutant removal effectiveness is enhanced when trees are close to the pollutant source, or are located where pollutant concentration is high (Beckett et al., 1998; Freer-Smith et al., 2005).

Hirabayashi et al. (2012) developed a grid-based prototype of i-Tree Eco, hereafter referred to as $iTreeEco_D$, where input temperature, leaf area index (LAI), and air pollutant concentrations are spatially distributed, while other meteorological parameters are lumped over the modeling domain. A couple of issues arise when implementing $iTreeEco_D$. The model's multiple regression temperature equation was derived for Baltimore, MD using long-term

* Corresponding author.
E-mail addresses: mtcabara@syr.edu, mticabaraban@gmail.com (M.T.I. Cabaraban).

0269-7491/$ – see front matter © 2013 Elsevier Ltd. All rights reserved.
http://dx.doi.org/10.1016/j.envpol.2013.01.006

data from the Baltimore Ecosystem Study (BES, 2012). A similar model could be used to estimate temperature patterns outside of Baltimore, although the regression coefficients may change for different regions of study. This change will require data from a high-density network of meteorological stations for long observation periods. Moreover, the Gaussian model applied in iTreeEco$_D$ is typically used to simulate the transport of non-reactive gaseous pollutants and may be unsuitable for estimating concentrations of highly reactive pollutants like nitrogen dioxide (NO_2) and secondary pollutants like fine particulate matter (PM).

In this study, the results obtained by Hirabayashi et al. (2012) were expanded to consider the effects of three factors on simulated dry deposition to urban trees. A mesoscale meteorological model was used to obtain near-surface (2-m) temperature and LAI fields, and a photochemical air quality model was used to obtain surface-level concentration fields. The impacts of these estimates on output from the urban-scale dry deposition simulation were examined. The goal of this study was not to validate model performance, but to investigate the degree to which variations in model inputs would affect estimates of dry deposition of air pollutants on vegetative surfaces.

2. Materials and methods

2.1. Case study – Baltimore, MD

The case study is for the Baltimore metropolitan area in Maryland for the time period from July 27 to 29, 2005. The gaseous pollutant of interest is NO_2, typically a local-scale pollutant, in that it is formed by combustion from local sources like traffic, industry, power plants, and inland waterway shipping. This gas was chosen since its presence in the atmosphere can affect ozone (O_3) or secondary PM (Seinfeld and Pandis, 2006).

Baltimore has an area of 210 km^2, 42 km^2 (20%) of which is urban tree canopy (Galvin et al., 2006). Among the land use categories, high-intensity urban areas (22% of total area), medium-intensity urban areas (28% of total area), and agricultural lands (4% of total area) have relatively low tree cover. A large concentration of industrial, commercial, power plants, and waste treatment and disposal facilities are sited in the southern district of the city, where residential neighborhoods are also located.

2.2. Description of the modeling systems

iTreeEco$_D$ integrates calculation tools to process and generate raster data of three input parameters: temperature, LAI, and air pollutant concentrations. Simplifying assumptions regarding these three iTreeEco$_D$ inputs are described in more detail elsewhere (Hirabayashi, 2009; Hirabayashi et al., 2012). iTreeEco$_D$ assumes fixed values of fractional tree cover and LAI across a defined land use type. Here, LAI is defined as the total one-sided area of green canopy elements over the ground projected canopy area (Hirabayashi et al., 2012; Liang et al., 2005). The detailed approach to calculate pollutant flux (F_p) in iTreeEco$_D$ is given in Hirabayashi et al. (2011b).

To improve the spatial modeling of the impacts of vegetation on air quality in urban areas, iTreeEco$_D$ was coupled to a regional air quality model. The US Environmental Protection Agency's (EPA's) Community Multiscale Air Quality (CMAQ) model was used in this study to estimate ambient pollutant concentration (C_p). CMAQ (Byun and Schere, 2006) is a three-dimensional Eulerian model that accounts for emissions, horizontal and vertical advection, eddy diffusion, cloud mixing, gas-phase chemical transformations, aqueous-phase chemical reactions, and aerosol processes.

The Weather Research and Forecasting (WRF) model was used to generate the hourly wind, temperature, humidity, mixing depth, and solar insolation fields required by CMAQ. WRF (Skamarock et al., 2008) is a mesoscale numerical weather prediction system developed by the National Oceanic and Atmospheric Administration (NOAA), and is maintained by the National Centers for Environmental Prediction (NCEP).

WRF, CMAQ, and iTreeEco$_D$ were combined using a loose coupling scheme, refering to the technique of integrating models at the input or output data level (Lieber and Wolke, 2008; Lilburne, 1996). Geographic information system (GIS) was used to extract and convert the binary network Common Data Form (netCDF) output files from WRF and CMAQ into raster datasets required by iTreeEco$_D$, which calculated and generated maps of dry deposition velocities (V_d) and F_p. WRF was used to output hourly gridded temperature and time-invariant LAI, and CMAQ to generate hourly gridded C_p. The LAI, temperature, and C_p fields were then used for dry deposition calculations in iTreeEco$_D$.

2.3. Model setup

2.3.1. iTreeEco$_D$ model simulations

Hourly meteorological data for iTreeEco$_D$ temperature, C_p, and dry deposition calculations were obtained from NOAA's National Climatic Data Center (NCDC, 2007). LAI calculations used the same values for leaf area and tree cover percentages for Baltimore as those used by Hirabayashi et al. (2011a, 2012), which were obtained from field sampled data gathered in 2004. Dry deposition calculations were limited to periods of no rain and with wind speed >0 m s^{-1}; periods not satisfying these conditions were omitted from further analyses.

2.3.2. WRF model simulations

WRF version 3.3 was implemented on two nested grids shown in Fig. 1. WRF was run for the 1.5 km domain using initial and boundary conditions from NCEP's $1°\times1°$ resolution Global Forecast System model analysis data with 6-h intervals (UCAR, 2007). The 1.5-km run provided the initial and boundary conditions for the 0.5 km run. The simulations used a 3-day spin up (i.e. the first three days of model output were discarded from the data analysis). Analyses were done for the period from July 27 to 29, 2005.

The WRF runs used land cover types derived from the Global Land Cover Characteristics (GLCC) (Loveland et al., 1991), which were created at a 1-km horizontal resolution using Advanced Very High Resolution Radiometer (AVHRR) satellite images from April 1992 to March 1993, and from the 30-m NLCD 2001. Incorporating the NLCD 2001 into the WRF framework allowed for evaluating the effects of different land cover data on the WRF estimates of LAI and near-surface temperature.

In succeeding discussions, the WRF simulation that used the GLCC land cover is referred to as WRFG, and that which used the NLCD land cover as WRFN. Using the coupled WRF/Noah land surface model (LSM)/Urban Canopy Model (UCM) system in WRFN necessitated fine-tuning the vegetation and urban parameters for the four developed land use types according to available information for Baltimore. Green vegetation fraction was derived from the same 1-km AVHRR product as for the GLCC, using the normalized difference vegetation index data for each land cover type (Liang et al., 2005; Zeng et al., 2000).

2.3.3. CMAQ model simulations

CMAQ version 4.7.1 was configured to utilize all 28 layers from the input meteorology. Anthropogenic and biogenic emissions datasets for CMAQ were generated by the Sparse Matrix Operator Kernel Emissions (SMOKE) modeling system version 2.6 (SMOKE, 2010). Meteorological outputs from the WRF simulations were processed to create model-ready inputs for CMAQ using the Meteorology–Chemistry Interface Processor (MCIP) version 3.6 (Otte et al., 2005).

Additional information about the models and model configurations are given in the Supplementary material.

2.4. Comparison methodology

To investigate the impact of varying model inputs on iTreeEco$_D$'s dry deposition estimates, six simulations were conducted. The first simulation (base case; S1) used output from built-in iTreeEco$_D$ (i.e. temperature, LAI, NO_2 concentration) calculation

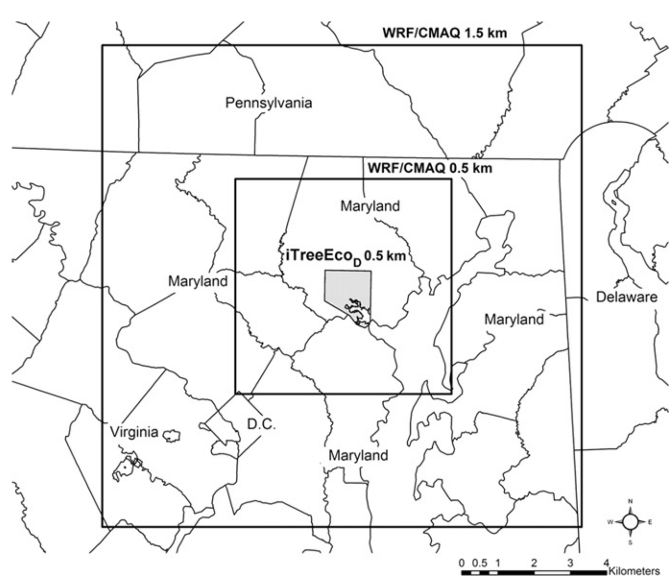

Fig. 1. Modeling domain showing locations of the WRF, CMAQ, and iTreeEco$_D$ grids.

tools to obtain estimates from the iTreeEco$_D$ dry deposition calculation tool. The second (S2) and third (S3) simulations differ from S1 by using LAI fields from WRFG and WRFN, respectively. The fourth (S4) and fifth (S5) simulations differ from S1 by using temperature fields from WRFG and WRFN, respectively. The sixth simulation (S6) differs from S1 by using CMAQ NO_2 concentration (C_{NO_2}) fields. iTreeEco$_D$ and MCIP/CMAQ differ in their approaches to parameterize V_d. Hence, a seventh simulation (S7) was conducted to assess differences in dry deposition estimates from the two models resulting from parameterization differences.

Note that the iTreeEco$_D$ domain is considerably smaller than the WRF and CMAQ domains, covering only metropolitan Baltimore. Land cover, LAI, temperature, and NO_2 concentration in netCDF extracted from WRF or CMAQ were converted to raster data layers, georeferenced to use the same geographic coordinate system as the raster layers from the iTreeEco$_D$ tools, and clipped to the iTreeEco$_D$ domain. Carrying out these raster operations introduced distortions inherent in changing map projections and created when resampling cell values (Seong, 2003; Steinwand et al., 1995; Yeh and Li, 2006).

Examination of simulation results uncovered the effects of different temperature, LAI, and C_{NO_2} inputs on estimated dry deposition. Model-to-measurement and model-to-model comparisons were considered (Lutman et al., 2004; Smyth et al., 2009). Model performance (EPA, 2007) was evaluated using:

$$\text{mean bias(MB)} = (1/N)\sum(\text{Mod}_i - \text{Obs}_i), \quad (1)$$

$$\text{normalized mean bias(NMB)} = \left(\sum(\text{Mod}_i - \text{Obs}_i)\Big/\sum\text{Obs}_i\right)*100, \quad (2)$$

and index of agreement (O'Neill and Lamb, 2005)

$$(\text{IOA}) = 1 - \left\{\sum(\text{Mod}_i - \text{Obs}_i)^2\Big/\sum(|\text{Mod}_i - \text{Obs}_{\text{ave}}| + |\text{Obsi} - \text{Obs}_{\text{ave}}|)^2\right\} \quad (3)$$

where N is number of measurements, Mod are modeled values, Obs are measured values, and Obs_{ave} are the average measured values.

There is only one meteorological station and one NO_2 monitoring station in metropolitan Baltimore. Therefore it was not possible to quantify biases in the temperature and C_{NO_2} estimates at other locations except at the monitoring sites. Additionally, dry deposition estimates could not be directly evaluated due to a lack of measurements in the study area.

Hourly estimates of temperatures, C_{NO_2} and NO_2 deposition fluxes (F_{NO_2}) were averaged over all modeled hours. The resulting temporally-averaged WRF temperature and CMAQ C_{NO_2} spatial plots were subtracted from similar spatial plots of iTreeEco$_D$ temperatures and C_{NO_2}, respectively, and the differences used as a measure of the relative divergence of the WRF and CMAQ datasets from the iTreeEco$_D$ datasets. Spatial plots for land cover and LAI were similarly compared. Spatial plots of modeled hourly temperatures, C_{NO_2} and F_{NO_2} were averaged over the modeling domain for each modeled hour, and the diurnal patterns compared. This comparison was conducted to uncover the variability in estimated F_{NO_2} associated with changes in land cover, LAI, temperature, and C_{NO_2} inputs. Only the temporal plot of F_{NO_2} is presented.

Fractional tree cover and fractional green vegetation cover are used interchangeably in ensuing discussions and, for brevity, are referred to as f_g. It should be emphasized that f_g are defined differently in iTreeEco$_D$ and WRF. Whereas all types of vegetation contributed to the f_g values in WRF, only trees and shrubs contributed to the f_g values in iTreeEco$_D$.

Average daily F_{NO_2} (mg m^{-2} d^{-1}) was obtained as the sum of hourly F_{NO_2} for all modeled hours divided by the number of modeling days. Hourly NO_2 removal (R_{NO_2}) across the modeling domain was calculated by multiplying the hourly F_{NO_2} by f_g. The hourly R_{NO_2} was summed over all modeled hours of the day to obtain the total daily R_{NO_2} (kg).

3. Results and discussion

Table 1 shows R_{NO_2} estimated by each of the seven simulations. Disparities in R_{NO_2} per simulation are due to variations in input parameters. S1, S4, and S5 had nearly the same average daily F_{NO_2}. S2 and S3 estimated the largest total R_{NO_2} among the simulations. S7 estimated the lowest average daily F_{NO_2} and the lowest daily R_{NO_2}.

3.1. iTreeEco$_D$ base case simulation (S1)

Fig. 2a presents land cover applied to the base case iTreeEco$_D$ simulation. iTreeEco$_D$ used two vegetated classes with mixed land features (forest/wetland and pasture/barren/cultivated land) and four urban-related classes (developed open space, developed low intensity, developed medium intensity, and developed high intensity).

Table 1
NO_2 removal by dry deposition to trees estimated by iTreeEco$_D$ (S1, S2, S3, S4, S5, and S6) and CMAQ (S7) in Baltimore, MD from July 27 to 29, 2005. Sn, where $n = 1$ to 7, represents the simulation number. The seven simulations in this study each made use of different input fields for dry deposition calculations.

	S1	S2	S3	S4	S5	S6	S7
Green vegetation fraction, f_g							
Min	0.09	0.00	0.00	0.09	0.09	0.09	0.00
Mean	0.20	0.59	0.62	0.20	0.20	0.20	0.59
Max	0.65	0.66	0.67	0.65	0.65	0.65	0.66
Std. dev.	0.15	0.14	0.09	0.15	0.15	0.15	0.14
Average daily NO_2 flux, mg m^{-2} d^{-1}							
Min	1.88	1.86	0.35	1.88	1.88	0.53	0.00
Mean	2.84	2.91	2.60	2.84	2.83	3.40	1.50
Max	6.63	6.23	6.62	6.62	6.62	8.70	3.40
Std. dev.	0.68	0.46	0.80	0.68	0.68	1.43	0.89
Total NO_2 removal, kg							
July 27	132.16	370.78	350.50	132.14	131.98	113.78	29.44
July 28	154.64	437.70	415.24	154.64	154.50	136.20	36.13
July 29	95.12	273.18	259.74	95.03	94.77	200.48	46.89
Total	381.92	1081.66	1025.48	381.81	381.25	450.46	112.46

iTreeEco$_D$ estimated high LAI values in patches of developed, open area ($f_g = 0.215$, LAI = 7) and in forest/wetland ($f_g = 0.652$, LAI = 5.24). Leaf area was larger for forest/wetland (62.4 km^2) than for developed, open area (48.6 km^2) by a factor of around 1.3. Estimated tree cover was also larger for forest/wetland (11.9 km^2) than for developed, open space (6.9 km^2) by a factor of around 1.7. Hence, estimated LAI was larger for developed, open area than for forest/wetland. Low LAI values were found in developed medium- ($f_g = 0.128$, LAI = 3.37) and high-intensity ($f_g = 0.092$, LAI = 2.91) areas. iTreeEco$_D$ average LAI across the modeling domain was 4.11 (std. dev. = 1.51). LAI values reported here are consistent with those for Baltimore summer conditions (Hirabayashi et al., 2011a; 2012) and for different land cover types (Asner et al., 2003).

As shown in Fig. 3a, iTreeEco$_D$ estimated the highest temperatures in the vicinity of the bay, extending to the city center. A temperature gradient was observed with the lowest temperature (24.1 °C) found in cells located at the western and northwestern edges, rising to 27 °C at the center of the modeling domain.

Fig. 4a presents the spatial distribution of iTreeEco$_D$-modeled C_{NO_2}. The plot shows the largest C_{NO_2} (14–19.2 ppb) were located downwind of highway cells, indicating a significant contribution of mobile sources to the modeled C_{NO_2}.

The temporal variation in S1 F_{NO_2} is demonstrated in Fig. 5. F_{NO_2} were relatively large (0.11–0.27 mg m^{-2} h^{-1}) during daytime, and around 14–20% of daytime values during nighttime. S1 estimated the highest F_{NO_2} (0.89–1.7 mg m^{-2} h^{-1}) in patches of forest/wetland cells, which were regions with high LAI, relatively high temperatures (>23 °C) and, due to their proximity to major roadways, high C_{NO_2} (30–37.3 ppb). F_{NO_2} were moderately high (0.35–1.03 mg m^{-2} h^{-1}) near major highways, where the model estimated moderately high LAI (3.37–5.24), low temperatures (<23 °C), and moderately high C_{NO_2} (12.9–14.1 ppb). Low F_{NO_2} were found in cells with low C_{NO_2} (<12.4 ppb) and relatively low temperatures. The ranges of S1 F_{NO_2} are consistent with values reported in Hirabayashi et al. (2012).

3.2. Effect of alternate land cover datasets on LAI and F_{NO_2}

In this section, comparisons are made between S1 and S2, and between S1 and S3. Because land cover type was used to attribute values to f_g and LAI in iTreeEco$_D$, differences in the land cover datasets are also discussed.

The disparities in the land cover datasets used in the iTreeEco$_D$ and WRFG simulations are attributed to differences in the spatial,

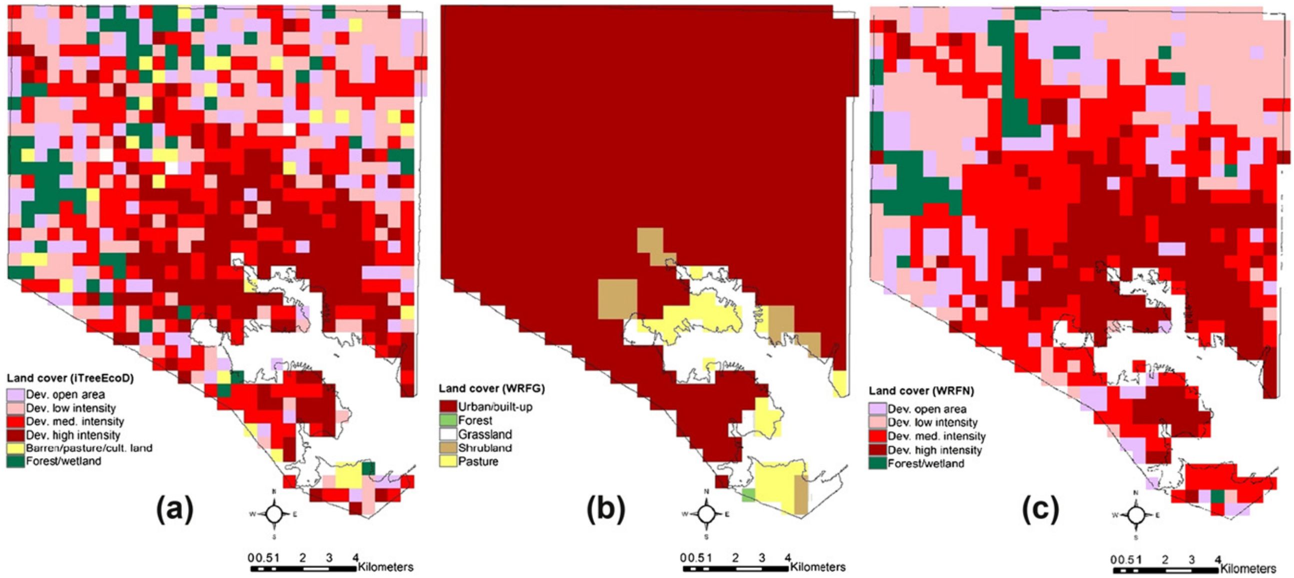

Fig. 2. Land cover data (a) obtained from NLCD 2001 (S1, S4, S5, and S6); (b) extracted from WRF using GLCC (S2 and S7); and (c) extracted from WRF using NLCD (S3).

temporal, and spectral resolution of the Landsat and AVHRR data from where the NLCD and GLCC data, respectively, were derived. Disagreements in the land cover maps are also attributed to differences in classification schemes. As shown in Fig. 2b, WRFG identified four vegetated classes (forest, grassland, shrub land, and pasture) and one urban-related class (urban and built-up land). The WRFG land cover map shows that large patches of shrub land and pasture were located adjacent to the bay, while iTreeEco$_D$ showed that barren/pasture/cultivated land was interspersed with developed and forest/wetland cells. With WRFG, urban and built-up land comprises more than 90% of Baltimore.

According to the iTreeEco$_D$ land cover dataset, around 86% of the modeling domain was developed, in contrast to the 91.5% in WRFN. More than 65% of iTreeEco$_D$ forest/wetland was covered by WRFN developed land, and iTreeEco$_D$ pasture/barren/cultivated land was missed in WRFN (Fig. 2c). Differences between the land cover maps used in iTreeEco$_D$ and in WRFN could be attributed to information losses related to the conversion of data formats and map projections that were carried out to prepare the dataset (Dixon and Earls, 2009; Yeh and Li, 2006). For example, information could be lost through resampling of the 30-m resolution NLCD data to 0.5 km resolution when it was integrated into the WRF framework.

WRFG estimated an LAI of 4.29 for urban and built-up land ($f_g = 0.564–0.658$). LAI estimates for iTreeEco$_D$ forest/wetland were reduced by a factor of 1.1–1.4 in WRFG. Conversely, WRFG-estimated LAI for iTreeEco$_D$ developed medium- and high-intensity cells were increased by a factor of around 1.2 to 1.5. Overall, WRFG LAI averaged across the domain (mean = 4.05, std. dev. = 0.23) was not much different from iTreeEco$_D$'s.

LAI values were reduced for forest/wetland (f_g = 0.49 to 0.67, LAI = 2.43–4.74) by a factor of 1.1–2.2 and for developed open space (f_g = 0.57 to 0.67, LAI = 1.00–2.64) by a factor of up to 7 in WRFN when compared to iTreeEco$_D$. Alternatively, WRFN-estimated LAI for developed medium- (f_g = 0.30 to 0.69, LAI = 2.76–4.29) and high-intensity (f_g = 0.32 to 0.67, LAI = 3.05–4.29) areas increased by a factor of up to 1.5 in comparison with iTreeEco$_D$. WRFN LAI (mean = 3.60, std. dev. = 0.32) was around 12% lower than iTreeEco$_D$ LAI across the domain.

WRF f_g values were generally higher than iTreeEco$_D$'s because of the contribution of other green canopy components such as grasses, resulting in discrepancies in estimated LAI. These discrepancies were further propagated in subsequent dry deposition calculations, resulting in the divergence in hourly F_{NO_2} and R_{NO_2} between S1 and S2, and between S1 and S3.

The diurnal variations of F_{NO_2} in S1 and S2 are similar (Fig. 5), with S2 daytime F_{NO_2} only around 2% larger than S1's. In S2, the distribution of F_{NO_2} resembled the spatial pattern of C_{NO_2} (Fig. 4a) and F_{NO_2} in S1. As seen in Table 1, using WRFG-derived LAI as input in S2 did not considerably change the average daily F_{NO_2}. However, S2 total R_{NO_2} were larger than S1's by a factor of 2.8, mainly due to the larger f_g values used in S2 in comparison with S1.

The diurnal distributions of S1 and S3 F_{NO_2} followed a similar pattern (Fig. 5), although S3 daytime F_{NO_2} were lower than S1's by around 8%. Similar to S1 and S2, S3 F_{NO_2} were larger in cells where C_{NO_2} were high. Although S1 and S3 each have the same average daily F_{NO_2}, the use of WRFN-derived LAI as input in S3 reduced the daily F_{NO_2} by a factor of 1.1. Lower LAI in S3 resulted in a decrease in estimated V_d, which had been shown to have a near linear relationship with LAI for NO_2 (Hirabayashi et al., 2011a). Additionally, S3 calculated larger R_{NO_2} than S1, due to larger f_g values used in S3, particularly for the developed land use types.

3.3. Effect of alternate temperature on F_{NO_2}

The temperature fields from WRFG and WRFN were compared with point measurements taken from the single meteorological station located in an urban cell in Baltimore. The effects of changes in temperature inputs on NO_2 deposition were assessed by comparing S1 and S4, and S1 and S5.

Table 2 shows summary statistical measures for modeled temperatures for the study domain. Both simulations were not able to capture the high temperature value (37.2 °C) at 16 LST of July 27. Modeled temperatures showed daytime (06–20 LST) and nighttime (00–05 LST and 21–23 LST) cold biases. The resulting overall cold biases of −1.2 °C for WRFG and −7.4 °C for WRFN might be due to an inadequacy of the heat and moisture transport parameterization in the YSU scheme to entrain warmer and drier air into the planetary boundary layer, similar to the findings of Hu et al. (2010) and Misenis and Zhang (2010). The Noah LSM might have overestimated the differences between land and water temperatures, especially during nighttime. In both simulations, temperatures

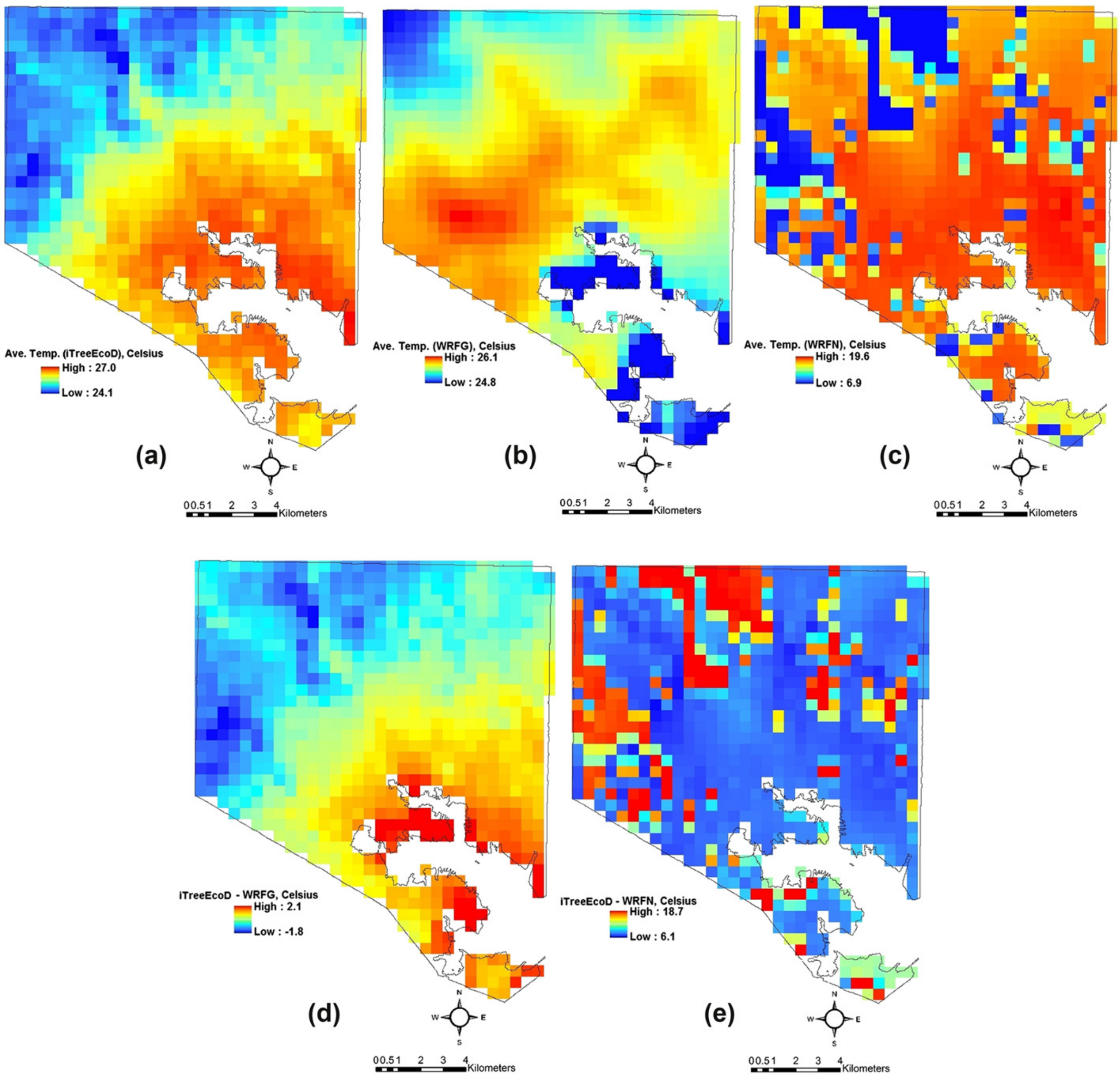

Fig. 3. Spatial plots of time-averaged 2-m temperatures (°C) modeled by the (a) iTreeEco$_D$ (S1, S2, S3, and S6), (b) WRFG (S4 and S7), and (c) WRFN (S5); and differences between iTreeEco$_D$- and (d) WRFG- and (e) WRFN-modeled 2-m air temperatures for Baltimore, MD.

decreased very sharply in the evening of the second day until the early morning hours of the third day, resulting in differences with observations >3 °C in WRFG and >10 °C in WRFN. These large temperature differences, particularly in the WRFN, produced the observed variability in the NMB values.

Fig. 6 shows a damped diurnal cycle of temperatures estimated by the WRFG and WRFN simulations in Baltimore. The diurnal variations were reproduced by WRFG with good accuracy, which is reflected in the model's overall IOA of 0.90. Bulk parameterization used in the WRFG include a roughness length of 0.8 m, a surface albedo of 0.15 to represent radiation trapping in urban canyons, a volumetric heat capacity of 3.0 MJ m^{-3} C^{-1}, and a thermal conductivity of 3.24 W m^{-1} C^{-1} to represent the large heat storage in urban buildings and roads. The use of these parameter values might have suppressed latent heat flux while enhancing sensible heat and storage heat fluxes (Lee et al., 2011), resulting in relatively high WRFG temperatures in urban cells.

WRFN did not perform as well as WRFG, with an overall IOA of 0.48. The underestimation of temperatures was grossly exacerbated in WRFN, probably due to the low urban fraction (λ_u) used for low-intensity ($\lambda_u = 0.76$) and medium-intensity ($\lambda_u = 0.81$) developed classes, which were derived from available information for Baltimore. Similar findings were reported by Salamanca et al. (2011), indicating that further improvements on surface parameterization are required for urban classes (Lee et al., 2011). Performance statistics for WRFG and WRFN temperatures (Table 2) indicate the adequacy of the bulk parameterization in WRFG to estimate near-surface temperature.

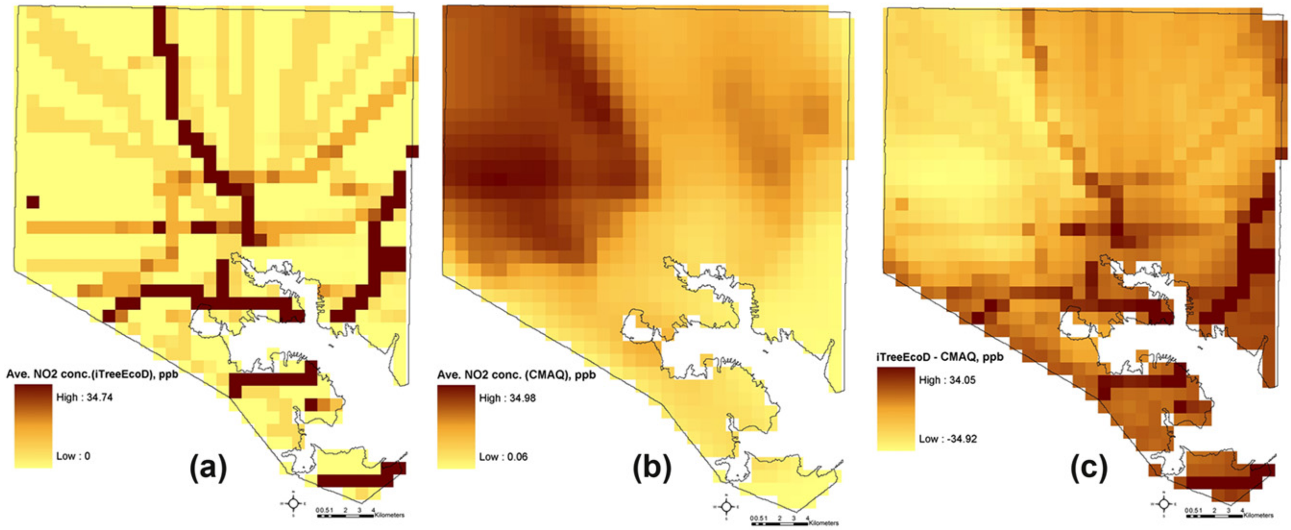

Fig. 4. Spatial plots of time-averaged (a) iTreeEco$_D$- (S1, S2, S3, S4, and S5) and (b) CMAQ-modeled (S6 and S7) NO_2 concentration (ppb), and (c) the differences in these concentrations for Baltimore, MD.

Fig. 3b shows the spatial plot of time-averaged WRFG temperatures. The map demonstrates a thermal gradient that progressed from high-temperature urban cells near the city center. WRFG estimated higher temperatures (by up to 1.8 °C) than iTreeEco$_D$, in the western and northern suburban Baltimore (Fig. 3d), and lower temperatures (from 1.4 to 2.1 °C) in industrial cells south of the modeling domain and adjacent to the bay. On average, however, WRFG temperatures (mean = 25.7 °C, std. dev. = 0.3 °C) did not differ much from iTreeEco$_D$ temperatures (mean = 25.7 °C, std. dev. = 0.8 °C).

The WRFN temperature map (Fig. 3c) shows low temperatures (<10 °C) in developed open areas and in forest/wetland cells. WRFN temperatures were lower than WRFG's by up to 3.5 °C, predominantly in the vicinity of the city center. WRFN temperatures were generally lower than iTreeEco$_D$'s, with a difference of 11.7–18.7 °C in forest/wetland cells (Fig. 3e). Overall, WRFN temperatures (mean = 15.9 °C, std. dev. = 4.0 °C) were lower than iTreeEco$_D$ temperatures.

The different spatial patterns of temperature derived from iTreeEco$_D$, WRFG, and WRFN are a function of model construct and land cover. iTreeEco$_D$ adopted a regression model that allows for approximation of near-surface temperatures from a relationship that was fitted to data collected for Baltimore and neighboring areas, whereas WRFG and WRFN parameterized energy and moisture exchanges between the land surface and the atmosphere using the Noah LSM that incorporates urban features such as surface morphology, presence of impervious materials, and vegetation cover.

As shown in Fig. 5, the diurnal variations of F_{NO_2} in S4 and S5 are similar to S1, both in pattern and magnitude. The distribution of F_{NO_2} in S4 and S5 reflected the spatial pattern of C_{NO_2} (Fig. 4a) and F_{NO_2} in S1. As seen in Table 1, iTreeEco$_D$ average daily F_{NO_2} and total

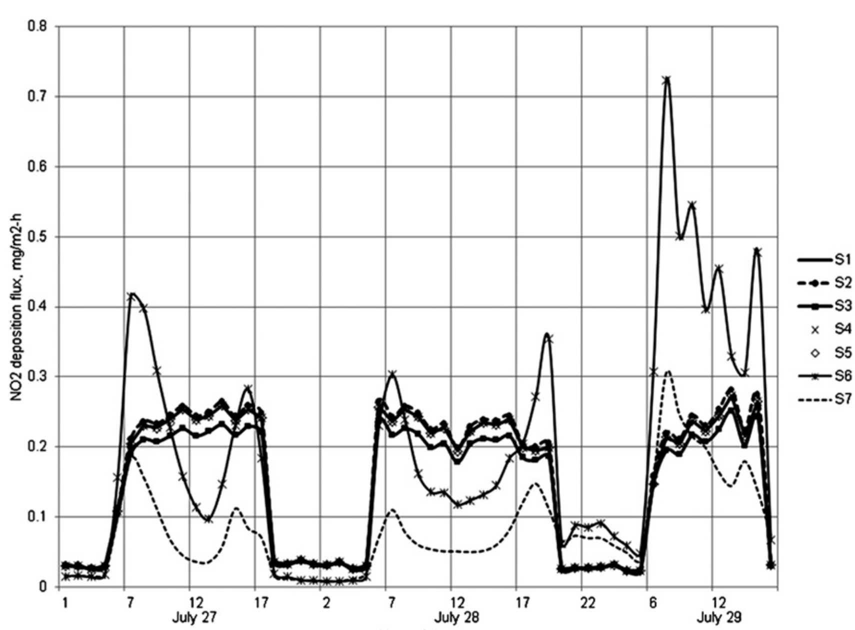

Fig. 5. Time-series comparison of modeled NO_2 hourly deposition fluxes averaged over all grid cells.

Table 2
WRF performance statistics for near-surface temperature at the weather monitor location from July 27 to 29, 2005.

	Min (°C)	Max (°C)		Mean (°C)	MB[a] (°C)	NMB[b] (%)	IOA[c]
Measured	21.7	37.2	All	26.8			
			Day	27.9			
			Night	25.5			
Modeled (WRFG)	19.2	35.4	All	25.6	−1.2	−4.6	0.90
			Day	26.5	−1.1	−3.8	0.92
			Night	24.0	−1.6	−6.1	0.84
Modeled (WRFN)	11.6	32.1	All	19.5	−7.4	−27.5	0.48
			Day	21.1	−6.5	−23.6	0.50
			Night	16.7	−8.8	−34.6	0.47

[a] MB, mean bias.
[b] NMB, normalized mean bias.
[c] IOA, index of agreement.

Table 3
CMAQ performance statistics for surface-level NO_2 concentrations at monitor location from July 27 to 29, 2005.

	Min (ppb)	Max (ppb)		Mean (ppb)	MB[a] (ppb)	NMB[b] (%)	IOA[c]
Measured	7.0	47.0	All	24.2			
			Day	22.1			
			Night	26.6			
Modeled (CMAQ)	2.5	39.1	All	10.8	−13.4	−55.4	0.56
			Day	10.1	−12.5	−55.5	0.60
			Night	12.0	−14.8	−55.3	0.49

[a] MB, mean bias.
[b] NMB, normalized mean bias.
[c] IOA, index of agreement.

R_{NO_2} were not affected by the use of WRFG- and WRFN-derived temperatures as input in S4 and S5, respectively. Temperature was used in V_d calculations. WRFG temperatures were similar in magnitude to iTreeEco$_D$'s, so that estimated V_d values were comparable between S1 and S4. The sensitivity analyses by Hirabayashi et al. (2011a) showed an increasing trend in V_d, up to about 20 °C when it reaches an optimum value. Further increases in temperature would cause V_d to decrease. It would appear that the ranges of temperatures in S1 and S5 yielded V_d values that are on opposite tails of this optimal curve, but are of similar magnitudes. Despite lower temperatures in S5 than in S1, V_d values for S1 and S5 were similar.

3.4. *Effect of alternate C_{NO_2} on F_{NO_2}*

The CMAQ C_{NO_2} fields were compared with point measurements taken from the single NO_2 monitoring station located in an urban cell in Baltimore. Comparisons were made between S1 and S6.

Table 3 shows the performance statistics for CMAQ-modeled C_{NO_2} for all hours. CMAQ underestimated hourly C_{NO_2}, with MB of −13.4 ppb and NMB of 55.4%. Biases were most substantial when C_{NO_2} were relatively high (between 00 and 06 LST of July 27, and between 13 and 23 LST of July 29), during which periods NO_2 dispersion might have been precluded by neutral to extremely stable atmospheric conditions characterized by overcast nighttime conditions and either light or absent surface winds. Modeled and measured NO_2 values have moderate agreement (IOA of about 0.6), with slightly better agreement during daytime than nighttime. Overall, the underestimation of C_{NO_2}, particularly during nighttime, may be due to an overestimation of NO_2 losses due to advection and diffusion. It would appear that NO_2 emissions and regeneration of NO_2 in the lowest layer did not sufficiently offset these transport losses, resulting in low estimated C_{NO_2}.

Fig. 7 shows the NO_2 time series comparisons between CMAQ results and observations at the monitoring station during the modeled period. Results show that CMAQ did well to capture the measurement pattern and the timing of peak C_{NO_2}, but underestimated NO_2 peak magnitudes.

The spatial distribution of time-averaged CMAQ C_{NO_2} (Fig. 4b) differs in magnitude and spatial variability from those estimated by iTreeEco$_D$ across the domain. High CMAQ-modeled C_{NO_2} were found in the vicinity of expressways and local roadways in the city's northwestern district. It can be observed from Fig. 4b that the mobile-source contribution to C_{NO_2} decreased from the city core area. CMAQ C_{NO_2} in these cells were higher (from 11.1 to 15.6 ppb)

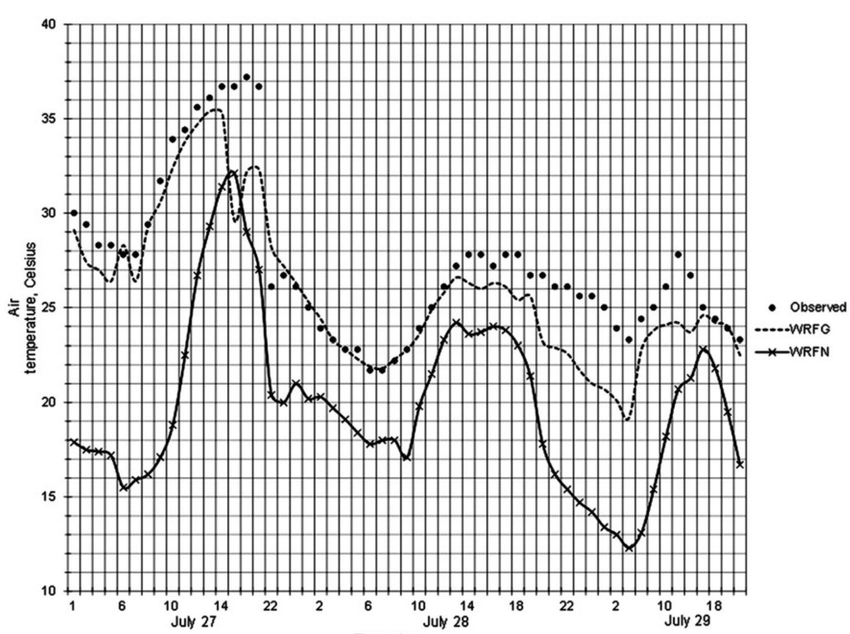

Fig. 6. Time-series comparison of measured and modeled near-surface temperature, in °C, from July 27 to 29, 2005 measured at the monitoring station in Baltimore.

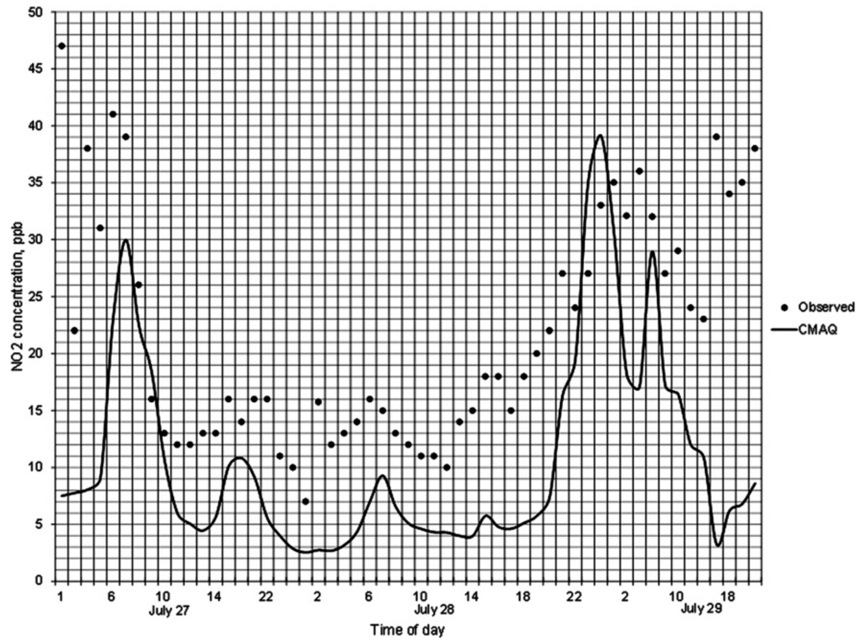

Fig. 7. Time-series comparison of measured and modeled surface-level NO_2 concentration, in ppb, from July 27 to 29, 2005 measured at the downtown Baltimore monitoring station.

than the iTreeEco$_D$ estimates for the same cells (Fig. 4c). On average, CMAQ C_{NO_2} (mean = 16.78 ppb, std. dev. = 9.6 ppb) were higher than iTreeEco$_D$ C_{NO_2} (mean = 2.76 ppb, std. dev. = 4.7 ppb). It is noted that in some hours during the simulation period (e.g. around noontime and hours before sunset from 17 to 20 LST), iTreeEco$_D$ estimated higher C_{NO_2} than CMAQ.

The differences in C_{NO_2} between these two models are most likely due to their treatment of chemical transformations of pollutants. The CB05 mechanism implemented in CMAQ attempts to capture all relevant gas-phase reactions that result in the formation and destruction of atmospheric pollutants leading to changes in their concentrations. The Gaussian model does not include a chemical transformation algorithm. C_{NO_2} might have been inaccurately estimated, especially if major chemical processes were important, e.g. the oxidation of nitric oxide by O_3 to form NO_2. The Gaussian and the CMAQ models also differ in their temporal disaggregation of annual emission data, as well as in their calculations and spatial allocation of mobile emissions.

Another potential reason for the differences in iTreeEco$_D$ and CMAQ outputs is in the models' handling of background concentrations. Background concentration is defined here as the concentration due to sources primarily outside the modeling domain, which are attributable to long-range transport and are not specified in the emission inventory. In CMAQ, temporally and spatially resolved concentration fields from the coarse-grid simulation provided background contributions from pollutants transported into the domain from the boundaries, whereas iTreeEco$_D$ considered the difference between measured and modeled values as the background concentration.

In addition to the above differences, the two models also differ in their approach to representing air flow and diffusion. The CMAQ model incorporates the spatial variation of topography, wind fields, and eddy diffusivities. The simplified physics of air transport in the Gaussian model are usually not representative of the complex turbulence and diffusion processes observed in urban air transport.

Fig. 5 reveals that the temporal variations of F_{NO_2} were different between S1 and S6, with higher peaks in S6. Both simulations show multiple peaks during all days of the simulation, with S6 showing more clearly defined daytime peaks. S6 F_{NO_2} shows a similar spatial pattern as C_{NO_2} (Fig. 4b). iTreeEco$_D$ average daily F_{NO_2} were increased by a factor of around 1.2 when CMAQ C_{NO_2} were used as an input in S6, due to higher C_{NO_2} in S6 than in S1. Moreover, R_{NO_2} was larger in S6 than S1 by a factor of around 1.2 as a result of higher C_{NO_2} in S6.

3.5. Comparison with CMAQ NO$_2$ dry deposition simulation (S7)

S7 used the meteorological field generated by WRFG, which were processed by MCIP, and applied as input to CMAQ. Compared to S1, S7 produced smaller average daily F_{NO_2} by a factor of 1.1–3.2, which was primarily due to lower V_d calculated from MCIP. S7 daytime V_d (mean = 0.23 cm s^{-1}, std. dev. = 0.05 cm s^{-1}) were lower than S1's (mean = 0.54 cm s^{-1}, std. dev. = 0.09 cm s^{-1}). The MCIP V_d fell at the lower end of the range (0.1–0.5 cm s^{-1}) reported in Lovett (1994), while the iTreeEco$_D$ V_d were at the upper end of or above this range. V_d in S1 and S7 were in accordance with compiled values in Holland et al. (2005).

The differences in V_d and F_{NO_2} could be explained partly by the differences in meteorological and emissions inputs, the f_g values used, the modeling of gaseous chemical transformations, the treatment of turbulence, and the parameterization of vertical transfer and surface uptake between the two models. Total R_{NO_2} was reduced by a factor of 3.4 in S7, due to lower V_d in S7 than in S1.

These comparisons of simulation results point to local C_p and f_g as major factors in pollutant removal, in agreement with findings elsewhere (Baldocchi et al., 1987; Escobedo and Nowak, 2009; Hirabayashi et al., 2011a; Jim and Chen, 2008; Nowak, 1994; Nowak et al., 2006; Sehmel, 1980). Results further suggest that the spatial distributions of C_p and f_g have much more influence on F_p calculations than the spatial distribution of air temperature in an urban setting such as Baltimore.

3.6. Uncertainties of the coupled system approach

As discussed elsewhere, there are several uncertainties of the iTreeEco$_D$ modeling system, which are a combination of uncertainties in input variables and model parameterization (Hirabayashi et al., 2012). Validation of dry deposition estimates suffered from the unavailability of dry deposition flux monitoring in Baltimore.

In addition, errors are introduced into the C_p estimation by the inherent uncertainty associated with the simplified processes within the Gaussian model. The Gaussian-based models in iTreeEco$_D$ are not capable of dealing with reactive pollutants, which could result in inaccurate estimation of C_p during periods when chemical transformations are important. Another approximation implied in the Gaussian model is that mean wind speeds are large enough so that upstream or longitudinal diffusion is negligible in comparison to mean transport. This assumption of constant mean transport in the horizontal plane could also be a source of model uncertainty, especially in urban areas where urban structures can significantly alter wind direction and speed (Neophytou et al., 2011).

The results of the simulations using the WRF/CMAQ/iTreeEco$_D$ coupled system are also subject to several uncertainties which should be noted. Land cover influences surface climate, and f_g is an important property to describe land surface processes and surface parameterization schemes used for climate and weather forecasting (Sertel et al., 2009). Accurate representation of vegetation in land surface schemes is therefore an important factor for weather prediction systems such as WRF. The deficiencies in vegetation characteristics (i.e. land cover classification and f_g) in the data sources used affected model simulations, causing uncertainties in the WRFG, WRFN, and CMAQ outputs. These uncertainties were propagated through the operations performed on these datasets in the iTreeEco$_D$ simulations, resulting in spatially variable uncertainties in F_{NO_2}. These estimates are subject to additional uncertainties from distortions resulting from processing (i.e. map reprojection and resampling) (Seong, 2003; Steinwand et al., 1995; Yeh and Li, 2006) of the WRFG, WRFN, and CMAQ netCDF fields to raster input files for iTreeEco$_D$.

4. Summary and conclusions

In this study, the effects of varying temperature, LAI, and C_{NO_2} inputs on iTreeEco$_D$ dry deposition estimates were investigated. The methodology involved loosely coupling WRF, CMAQ, and iTreeEco$_D$ using a set of procedures that included meteorological modeling in WRF, air quality modeling in CMAQ, and calculation of F_p in iTreeEco$_D$. GIS was used to preprocess meteorological and C_p fields for subsequent spatial analyses in iTreeEco$_D$. The comparative evaluation helped to identify differences in simulation results caused by differences in the models' parameterizations, processes, and numerical algorithms, and to reveal similarities and differences in the spatial patterns of F_{NO_2}. The simulation study was performed in Baltimore, MD for the end of July 2005. The strategy presented here demonstrated how the capabilities of WRF and CMAQ could be integrated with iTreeEco$_D$ in a loosely coupled system.

iTreeEco$_D$ was able to better describe spatial heterogeneity in LAI values than WRF, which could be attributed to model formulation and input. One would expect iTreeEco$_D$ LAI to be an improvement over those from WRF since they are based on a combination of both field plot data and more detailed land cover information. The GLCC data used in WRF are not current and may not be accurate for urban areas (Sertel et al., 2009). The incorporation of NLCD data in WRF provided a more detailed description of the spatial variation in estimated LAI than was provided by the WRFG simulation, although it was lower than the iTreeEco$_D$ LAI due to higher WRFN f_g values in comparison with iTreeEco$_D$ f_g values. The current version of i-Tree Eco focuses only on urban trees and shrubs. In future model development, f_g estimates in i-Tree Eco could include the contributions of other green canopy components.

The regression-based approach in iTreeEco$_D$ was shown capable to provide adequate estimates of the temporal and spatial distribution of temperatures in Baltimore (Heisler et al., 2007; Hirabayashi et al., 2012). However, the regression model does not capture the underlying physics driving the urban climate system, which might explain the model's fairly low correlation coefficient with measured data (Heisler et al., 2007). In contrast, WRF adopts a physics-based approach that explicitly considers land surface–atmosphere exchange. Bulk parameterization in WRFG was shown to produce sufficient estimates of temperature, while detailed urban parameterizations in the UCM in WRFN only served to impair near-surface temperature estimates (Salamanca et al., 2011).

This study has demonstrated the utility of WRF to generate LAI and temperature maps. This approach will be useful when field sampled data are not on hand to estimate a study area's leaf area and tree cover, and will be more advantageous than the temperature regression model in iTreeEco$_D$ in locations where long-term observations from multiple weather stations are unavailable. Estimates could be improved by using MODIS LAI and f_g data in WRF (Ke et al., 2012; Liang et al., 2005; Sea et al., 2011), which better reflect vegetation characteristics than the AVHRR-based climatology data currently used in WRF, thereby enhancing surface energy budgets within the Noah LSM with bulk urban parameterization.

The difference in the spatial pattern of C_{NO_2} from iTreeEco$_D$ and CMAQ was not unexpected, since the chemical mechanisms and the numerical algorithms for transport processes were different in the two models. The Gaussian model in iTreeEco$_D$, which is widely used to simulate concentrations of relatively nonreactive gases, requires the assumption of ideal and constant conditions, which rarely occur. A grid model that accounts for atmospheric chemical transformations would more appropriately model reactive air pollutants such as NO_2, O_3, and PM. Results from this analysis indicate that some changes to the air pollutant model within iTreeEco$_D$ may be warranted for reactive air pollutants. Moreover, the appropriate selection of background values could reduce uncertainties in estimating the spatial variation of air pollutant concentrations.

The iTreeEco$_D$ simulation using WRF temperature inputs produced F_{NO_2} that are similar both in magnitude and spatial pattern as those produced from using the regression-based temperature inputs. WRF-estimated LAI inputs to the iTreeEco$_D$ simulations resulted in large spatial changes in F_{NO_2} from those calculated using the built-in LAI calculation tool, and showed the highest fluxes in areas where C_{NO_2} were high. Using CMAQ-modeled C_{NO_2} in the iTreeEco$_D$ simulation also resulted in considerable disparity in the spatial distribution of F_{NO_2} when compared to estimates from using the Gaussian-based C_{NO_2} inputs, and showed gradients of F_{NO_2} that increased from the central commercial and eastern residential districts of Baltimore toward the industrial and residential districts west and south of the city.

The comparisons of the simulation results show that the use of different inputs from iTreeEco$_D$ calculation tools, WRF, and CMAQ introduced uncertainties into the dry deposition estimates because of the different assumptions used, errors in the available model inputs, and uncertainties related to raster data processing. Rather than suggesting that the use of one dataset resulted in more accurate estimates of dry deposition than the other, which was not possible to establish given the challenges in validating these datasets and the modeled dry deposition values, this study focused on the effects of the variability in model inputs on iTreeEco$_D$ estimates of dry deposition. This study lays the groundwork for future applications of iTreeEco$_D$ where detailed local-scale land cover, meteorological, or air pollutant concentration information may be unavailable.

Building on the results of this modeling demonstration, downwind C_p from emission sources need to be estimated more accurately to make reasonable F_p estimates. Future research will also investigate the spatial distribution of near-surface temperature and C_p under different atmospheric stability conditions. Such investigations will be useful in assessing the impacts of atmospheric stability on V_d and F_p.

Acknowledgment

The authors acknowledge the USDA Forest Service National Urban and Community Forestry Advisory Council (NUCFAC) and the Fulbright Foreign Student Program for partially funding this research.

Appendix A. Supplementary data

Supplementary data related to this article can be found at http://dx.doi.org/10.1016/j.envpol.2013.01.006.

References

Asner, G.P., Scurlock, J.M.O., Hicke, J.A., 2003. Global synthesis of leaf area index observations: implications for ecological and remote sensing studies. Global Ecology and Biogeography 12, 191–2005.
Baldocchi, D.D., Hicks, B.B., Camara, P., 1987. A canopy stomatal resistance model for gaseous deposition to vegetated surfaces. Atmospheric Environment 21, 91–101.
Beckett, K.P., Freer-Smith, P.H., Taylor, G., 1998. Urban woodlands: their role in reducing the effects of particulate pollution. Environmental Pollution 99, 347–360.
Baltimore Ecosystem Study (BES), 2012. http://www.beslter.org/ (accessed 15.10.08.).
Byun, D., Schere, K., 2006. Review of the governing equations, computational algorithms, and other components of the models-3 Community Multiscale Air Quality (CMAQ) modeling system. Applied Mechanics Reviews 59, 51–77.
Davidson, A.W., Barnes, J.D., 2002. In: Bell, J.N.B., Treshow, M. (Eds.), Air Pollutant – Abiotic Stress Interactions, second ed. John Wiley and Sons Ltd., West Sussex (Eng), p. 359.
Dixon, B., Earls, J., 2009. Resample or not?! Effects of resolution of DEM in watershed modeling. Hydrological Processes 23, 1714–1724.
Driscoll, C.T., Han, Y.J., Chen, C.Y., Evers, D.C., Lambert, K.F., Holsen, T.M., Kamman, N.C., Munson, R.K., 2007. Mercury contamination in forest and freshwater ecosystems in the Northeastern United States. BioScience 57, 17–28.
Environmental Protection Agency (EPA), 2007. Guidance on the Use of Models and Other Analyses for Demonstrating Attainment of Air Quality Goals for Ozone, $PM_{2.5}$, and Regional Haze, EPA-454/B-07–002, pp. 1–262. http://www.epa.gov/scram001/guidance/guide/final-03-pm-rh-guidance.pdf (accessed 05.04.10.).
Escobedo, F.J., Nowak, D., 2009. Spatial heterogeneity and air pollution removal by an urban forest. Landscape and Urban Planning 90, 102–108.
Fowler, D., 2002. In: Bell, J.N.B., Treshow, M. (Eds.), Pollutant Deposition and Uptake by Vegetation, second ed. John Wiley and Sons Ltd, West Sussex, England, pp. 43–67.
Freer-Smith, P., Beckett, K., Taylor, G., 2005. Deposition velocities to *Sorbus aria*, *Acer campestre*, *Populus deltoides X trichocarpa* 'Beaupre', *Pinus nigra* and *X Cupressocyparis leylandii* for coarse, fine and ultra-fine particles in the urban environment. Environmental Pollution 133, 157–167.
Galvin, M.F., Grove, J.M., O'Neil-Dunne, J., 2006. A Report on Baltimore City's Present and Potential Urban Tree Canopy, pp. 1–17. http://www.fs.fed.us/nrs/utc/reports/UTC_Report_BACI.pdf (accessed 04.07.11.).
Gurjar, B.R., Butler, T.M., Lawrence, M.G., Lelievel, J., 2008. Evaluation of emissions and air quality in megacities. Atmospheric Environment 42, 1593–1606.
Heisler, G., Walton, J., Yesilonis, I., Nowak, D., Pouyat, R., Grant, R., Grimmond, S., Hyde, K., Bacon, G., 2007. Empirical modeling and mapping of below-canopy air temperatures in Baltimore, MD and vicinity. In: Proceedings of the Seventh Urban Environment Symposium; September 10–13, 2007. American Meteorological Society, San Diego, CA, p. 7.
Hirabayashi, S., 2009. Coupling of Environmental Models and Geographic Information Systems (Doctoral dissertation). Available from Proquest Dissertations and Theses database (UMI 3354858).
Hirabayashi, S., Kroll, C.N., Nowak, D.J., 2011a. Component-based development and sensitivity analyses of an air pollutant dry deposition model. Environmental Modeling and Software 26, 804–816.
Hirabayashi, S., Kroll, C.N., Nowak, D.J., 2011b. I-tree Eco Dry Deposition Model Descriptions. http://www.itreetools.org/eco/resources/iTree_Eco_Dry_Deposition_Model_Descriptions_V1_1.pdf (accessed 15.02.12.).
Hirabayashi, S., Kroll, C.N., Nowak, D.J., 2012. Development of a distributed air pollutant dry deposition modeling framework. Environmental Pollution 171, 9–17.
Holland, E.A., Braswell, B.H., Sulzman, J., Lamarque, J., 2005. Nitrogen deposition onto the United States and Western Europe: synthesis of observations and models. Ecological Applications 15, 38–57.
Hopke, P.K., 2009. Contemporary threats and air pollution. Atmospheric Environment 43, 87–93.
Hu, X.M., Nielsen-Gammon, J.W., Zhang, F., 2010. Evaluation of three planetary boundary layer schemes in the WRF model. Journal of Applied Meteorology and Climatology 49, 1831–1845.
i-Tree, 2012. i–Tree Eco. http://www.itreetools.org/eco/ (accessed 20.01.12.).
Jim, C.Y., Chen, W.Y., 2008. Assessing the ecosystem service of air pollutant removal by urban trees in Guangzhou (China). Journal of Environmental Management 88, 665–676.
Ke, Y., Leung, L.R., Huang, M., Coleman, A.M., Li, H., Wigmosta, M.S., 2012. Development of high resolution land surface parameters for the Community Land Model. Geoscientific Model Development 5, 1341–1362.
Lee, S.H., Kim, S.W., Angevine, W.M., Bianco, L., McKeen, S.A., Senff, C.J., Trainer, M., Tucker, S.C., Zamora, R.J., 2011. Evaluation of urban surface parameterizations in the WRF model using measurements during the Texas Air Quality Study 2006 field campaign. Atmospheric Chemistry and Physics 11, 2127–2143.
Liang, X.Z., Choi, H.I., Kunkel, K.E., Dai, Y., Joseph, E., Wang, J.X., Kumar, P., 2005. Surface boundary conditions for mesoscale regional climate models. Earth Interactions 9, 1–28.
Lieber, M., Wolke, R., 2008. Optimizing the coupling in parallel air quality model systems. Environmental Modeling and Software 23, 235–243.
Lilburne, L., 1996. The integration challenge. In: Proceedings of the Spatial Information Research Center's 8th Colloquium; July 9–11, 1996. University of Otago, New Zealand, pp. 85–94.
Loveland, T.R., Merchant, J.W., Ohlen, D.O., Brown, J.F., 1991. Development of a land-cover characteristics database for the conterminous U.S. Photogrammetric Engineering and Remote Sensing 57, 1453–1463.
Lovett, G.M., 1994. Atmospheric deposition of nutrients and pollutants in North America: an ecological perspective. Ecological Applications 4, 629–650.
Lutman, E.R., Jones, S.R., Hill, R.A., McDonald, P., Lambers, B., 2004. Comparison between the predictions of a Gaussian plume model and a Langrangian particle dispersion model for annual average calculations of long-range dispersion of radionuclides. Journal of Environmental Radioactivity 75, 339–355.
Misenis, C., Zhang, Y., 2010. An examination of sensitivity of WRF/Chem predictions to physical parameterizations, horizontal grid spacing, and nesting options. Atmospheric Research 97, 315–334.
National Climatic Data Center (NCDC), 2007. Quality-controlled Climatological Data. http://cdo.ncdc.noaa.gov/qclcd/QCLCD (accessed 13.07.10.).
Neophytou, M., Gowardhan, A., Brown, M., 2011. An inter-comparison of three urban wind models using Oklahoma City Joint Urban 2003 wind field measurements. Journal of Wind Engineering and Industrial Aerodynamics 99, 357–368.
Nowak, D.J., 1994. Air Pollution Removal by Chicago's Urban Forest. In: General technical report NE-186, pp. 63–81. Radnor, PA.
Nowak, D.J., Crane, D.E., Stevens, J.C., 2006. Air pollution removal by urban trees and shrubs in the United States. Urban Forestry and Urban Greening 4, 115–123.
O'Neill, S.M., Lamb, B.K., 2005. Intercomparison between the Community Multiscale Air Quality model and CALGRID using process analysis. Environmental Science and Technology 39, 5742–5753.
Otte, T.L., Pouliot, G., Pleim, J.E., Young, J.O., Schere, K.L., Wong, D.C., Lee, P.C.S., Tsidulko, M., McQueen, J.T., Davidson, P., Mathur, R., Chuang, H.Y., DiMego, G., Seaman, N.L., 2005. Linking the Eta model with the Community Multiscale Air Quality (CMAQ) modeling system to build a national weather forecasting system. Weather and Forecasting 20, 367–384.
Parrish, D.D., Singh, H.B., Molina, L., Madronich, S., 2011. Air quality progress in North American megacities: a review. Atmospheric Environment 45, 7015–7025.
Salamanca, F., Martilli, A., Tewari, M., Chen, F., 2011. A study of the urban boundary layer using different urban parameterizations and high-resolution urban canopy parameters with WRF. Journal of Applied Meteorology and Climatology 50, 1107–1128.
Schlesinger, R.B., 2007. The health impact of common inorganic components of fine particulate matter (PM2.5) in ambient air: a critical review. Inhalation Toxicology 19, 811–832.
Sea, W.B., Choler, B., Beringer, J., Weinmann, R.A., Hutley, L.B., Leuning, R., 2011. Documenting improvement in leaf area index estimates from MODIS using hemispherical photos for Australian savannas. Agricultural and Forest Meteorology 151, 1453–1461.
Sehmel, G.A., 1980. Particle and gas dry deposition: a review. Atmospheric Environment 14, 983–1011.
Seinfeld, J.H., Pandis, S.N., 2006. Atmospheric Chemistry and Physics, second ed. John Wiley and Sons Ltd., Hoboken, NJ.
Seong, J.C., 2003. Modelling the accuracy of image data reprojection. International Journal of Remote Sensing 24, 2309–2321.
Sertel, E., Robock, A., Ormeci, C., 2009. Impacts of land cover data quality on regional climate simulations. International Journal of Climatology. http://dx.doi.org/10.1002/joc.2036.
Skamarock, W.C., Klemp, J.B., Dudhia, J., Barker, D.M., Gill, D.O., Duda, M.G., Huang, X.Y., Wang, W., Powers, J.G., 2008. A Description of the Advanced Research WRF Version 3, NCAR/TN-475+STR, 113 pp.
Smith, R.I., Fowler, D., Sutton, M.A., Flechard, C., Coyle, M., 2000. Regional estimation of pollutant gas dry deposition in the UK: model description, sensitivity analyses and outputs. Atmospheric Environment 34, 3757–3777.

Sparse Matrix Operator Kernel Emissions (SMOKE), 2010. http://www.smoke-model.org/version2.6/index.cfm (accessed 15.09.10.).
Smyth, S.C., Jiang, W., Roth, H., Moran, M.D., Makar, P.A., Yang, F., Bouchet, V.S., Landry, H., 2009. A comparative performance evaluation of the AURAMS and CMAQ air-quality modelling systems. Atmospheric Environment 43, 1059–1070.
Steinwand, D.R., Hutchinson, J.A., Snyder, J.P., 1995. Map projections for global and continental data sets and an analysis of pixel distortion caused by reprojection. Photogrammetric Engineering and Remote Sensing 61, 1487–1499.
University Corporation for Atmospheric Research (UCAR), 2007. NCEP FNL Operational Model Global Tropospheric Analyses. CISL Research Data Archive 2010. http://dss.ucar.edu/datasets/ds083.2/data/ (accessed 25.08.10.).
Yeh, A.G.O., Li, X., 2006. Errors and uncertainties in urban cellular automata. Computers, Environment and Urban Systems 30, 10–28.
Zeng, X., Dickinson, R.E., Walker, A., Shaikh, M., DeFries, R.S., Qi, J., 2000. Derivation and evaluation of 1-km global fractional vegetation cover data for land modeling. Journal of Applied Meteorology 39, 826–839.